ResearchGate

See discussions, stats, and author profiles for this publication at: https://www.researchgate.net/publication/260240616

Active and Stable Liquid Water Innovatively Prepared Using Resonantly Illuminated Gold Nanoparticles

ARTICLE *in* ACS NANO · FEBRUARY 2014

Impact Factor: 12.88 · DOI: 10.1021/nn406403c · Source: PubMed

CITATIONS
4

READS
44

17 AUTHORS, INCLUDING:

Bing Joe Hwang
National Taiwan University of Science and T…
320 PUBLICATIONS **6,130** CITATIONS
SEE PROFILE

Fu-Der Mai
Taipei Medical University
46 PUBLICATIONS **427** CITATIONS
SEE PROFILE

Chun-Mao Lin
Taipei Medical University
52 PUBLICATIONS **882** CITATIONS
SEE PROFILE

Ming-Jer Lee
National Taiwan University of Science and T…
205 PUBLICATIONS **2,490** CITATIONS
SEE PROFILE

Available from: Ming-Jer Lee
Retrieved on: 02 February 2016

Active and Stable Liquid Water Innovatively Prepared Using Resonantly Illuminated Gold Nanoparticles

Hsiao-Chien Chen,[†] Bing-Joe Hwang,[‡] Fu-Der Mai,[†,§] Yu-Chuan Liu,[†,§,*] Chun-Mao Lin,[†] Hsien-Shou Kuo,[†] Duen-Suey Chou,[⊥] Ming-Jer Lee,[‡] Kuang-Hsuan Yang,[∥] Chung-Chin Yu,[¶] Jiun-Rong Chen,[#] Tsui-Yun Lo,[†] Hui-Yen Tsai,[†] Chih-Ping Yang,[▲] Chi Wang,[▲] Hsiao-Ting Hsieh,[▲] and John Rick[‡]

[†]Department of Biochemistry, School of Medicine, College of Medicine, Taipei Medical University, No. 250, Wu-Hsing Street, Taipei 11031, Taiwan, [‡]Department of Chemical Engineering, National Taiwan University of Science and Technology, No. 43, Sec. 4, Keelung Road, Taipei 10607, Taiwan, [§]Biomedical Mass Imaging Research Center and [⊥]Department of Pharmacology, School of Medicine, College of Medicine, Taipei Medical University, No. 250, Wu-Hsing Street, Taipei 11031, Taiwan, [∥]Department of Materials Science and Engineering and [¶]Department of Environmental Engineering, Vanung University, No. 1, Van Nung Road, Chung-Li City 32061, Taiwan, and [#]School of Nutrition and Health Sciences and [▲]Graduate Institute of Medical Science, College of Medicine, Taipei Medical University, No. 250, Wu-Hsing Street, Taipei 11031, Taiwan

ABSTRACT The properties of confined liquid water, or liquid water in contact with hydrophobic surfaces, are significantly different from those of bulk liquid water. However, all of water's commonly described properties are related to inert "bulk liquid water" which comprises a tetrahedral hydrogen-bonded network. In this work, we report an innovative and facile method for preparing small water clusters (SWCs) with reduced affinity hydrogen bonds by letting bulk water flow through supported Au nanoparticles (NPs) under resonant illumination to give NP-treated (AuNT) water at constant temperature. Utilizing localized surface plasmon resonance on illuminated Au NPs, the strong hydrogen bonds of bulk water can be disordered when water is located at the illuminated Au/water interface. The prepared SWCs are free of Au NPs. The energy efficiency for creating SWCs is ~17%. The resulting stable AuNT water exhibits distinct properties at room temperature, which are significantly different from the properties of untreated bulk water, examples being their ability to scavenge free hydroxyl and 2,2-diphenyl-1-picrylhydrazyl radicals and to effectively reduce NO release from lipopolysaccharide-induced inflammatory cells.

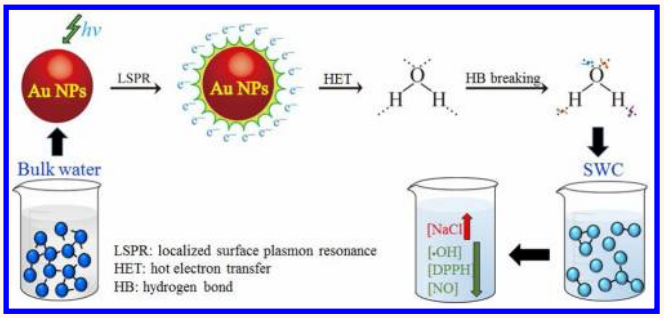

KEYWORDS: small water clusters · Au nanoparticles · resonant illumination · solubility · free radical

Because Au nanoparticles (NPs) possess well-defined localized surface plasmon resonance (LSPR) bands in the UV–near-IR regions, they are commonly used in surface-enhanced Raman scattering (SERS)[1,2] studies for improved diagnostic imaging and the photothermal ablation of tumors.[3] As shown in the literature,[4] a significant kinetic barrier opposes the direct thermal splitting of water at temperatures <2000 °C. Nevertheless, the photocatalytic generation of hydrogen and oxygen from water on the surface of Au-decorated TiO_2 NPs is practicable and efficient.[5] The role of water in living organisms, such as water sorption-induced swelling in plants,[6] has led to bioinspired polymer composites of polypyrrole and polyol-borate that exhibit sorption and desorption in water gradients for actuation.[7] In red corpuscles, aquaporin water channels are so selective that water passes through them to transfer nutrients and metabolites, while protons do not pass through.[8] Water can facilitate the oxidation of metals in the presence of dissolved oxygen[9] while also acting as a catalyst for radical gas-phase reactions.[10] Solid water (ice) has a nearly perfect tetrahedral symmetry around each water molecule, while liquid water with defects deviates from the

* Address correspondence to liuyc@tmu.edu.tw.

Received for review December 14, 2013 and accepted February 17, 2014.

Published online February 17, 2014
10.1021/nn406403c

© 2014 American Chemical Society

perfect tetrahedral symmetry of a hydrogen-bond network, thereby allowing it to play a central role in a vast number of chemical processes. Moreover, liquid water is able to form a flexible dynamic hydrogen-bonded network, in which hydrogen bonds are broken and formed at equilibrium on a picosecond time scale, thus making investigating its local structure challenging.[11] However, the O−H stretching frequency of water is very sensitive to the environment, thus making vibration-based spectroscopies, such as Raman scattering[12] and IR absorption,[13] suitable for examining water's hydrogen-bonded structure.

As reported by Ohsawa *et al.*,[14] acute oxidative stress, induced by inflammation, causes serious damage to tissues, while persistent oxidative stress is an acknowledged underlying cause of many common diseases, including cancer.[15] Their studies indicated that hydrogen can selectively reduce the hydroxyl radical, which is the most cytotoxic reactive oxygen species (ROS), but that hydrogen did not react with other ROS. Currently, because our molecular-level understanding of water is far from complete, all the known physical and chemical properties of water are based on "normal" bulk water. In this work, Au NP-treated (AuNT) water with weak hydrogen bonding was prepared by utilizing plasmonic absorption of light on resonantly illuminated Au NPs. The distinct properties and antioxidative activity of prepared AuNT water are shown in detail.

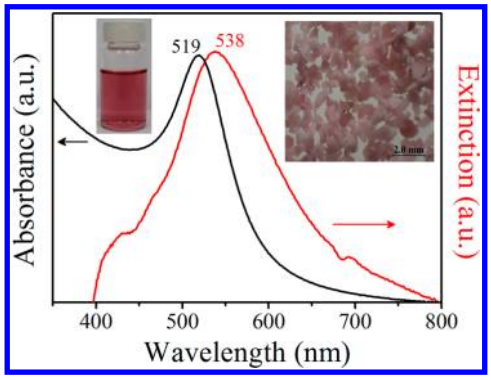

Figure 1. UV−vis absorption spectrum of Au NPs in solution (black line) and UV−vis extinction spectrum of Au NP-adsorbed ceramic particles (red line).

RESULTS AND DISCUSSION

Preparation of Water with Reduced Hydrogen Bonding. As shown in Figure 1, the surface plasmon resonant band of Au NPs in solution appears at 519 nm. This plasmon band's center is red-shifted to 538 nm and becomes broader over the whole visible light region when the Au NPs were adsorbed on ceramic particles. This characteristic LSPR of Au NPs adsorbed on ceramic particles indicates the effect of hot electron transfer (HET) for breaking the hydrogen bonds of bulk water which can be achieved under illumination with white light and further enhanced by wavelength-optimized resonant light. Figure 2A,B shows, respectively, the potential energy curve and the preparation of small water clusters (SWCs) with weak hydrogen bonding. The preparation of SWCs, free from Au NPs, is practicable under the illumination of a commonly available fluorescent lamp with full visible wavelength or alternatively under green-light-emitting diodes (LED, wavelength maxima centered at 530 nm). Throughout this work, unless stated otherwise, the AuNT water was prepared under the illumination of indoor fluorescent lamps.

Characterization of Water with Reduced Hydrogen Bonding. Figure 3 shows OH stretching Raman spectra with various pure water samples. The ceramic particle-treated (CPT) water was obtained by using similar preparation conditions to those used in the preparation of

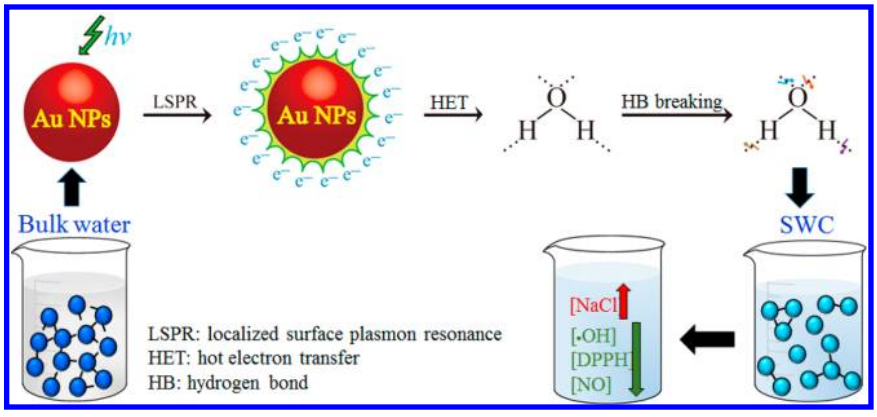

Figure 2. Schematics of the mechanism of the preparation of SWCs with reduced hydrogen bonding based on LSPR effect on Au NPs under resonant illumination and distinct property and antioxidative activity of prepared SWCs. The formation of SWCs occurs at the resonantly illuminated Au interface. In storage in the absence of Au NPs, both the forward reaction from bulk water to AuNT water and the corresponding reverse reaction from AuNT water to bulk water are slow due to huge activation energies required for both reactions. Therefore, the prepared SWC is temporarily trapped in a relatively stable state in an activation energy valley, in which it can persist in liquid water without reverting to normal hydrogen-bonding patterns observed in bulk water. The saturated solubility of NaCl in SWCs can be significantly increased. SWC itself can effectively scavenge free hydroxyl and DPPH radicals. Also, a SWC effectively reduces NO release from LPS-induced inflammatory cells.

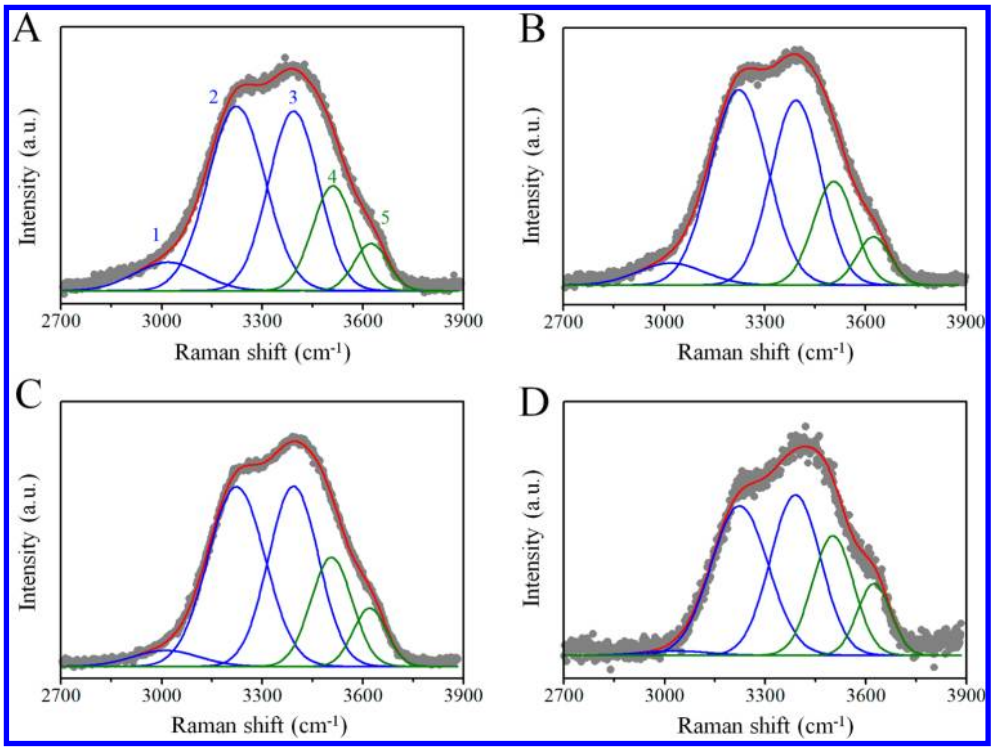

Figure 3. Raman spectra of OH stretching of various water: (A) DI water for reference. (B) Ceramic particle-treated (CPT) water, which was prepared under illumination of fluorescent lamps. (C) AuNT water, which was prepared under illumination of fluorescent lamps. (D) Super small water clusters (SWCs); this super SWC Raman spectrum was obtained by irradiating DI water-wetted ceramic-supported Au NPs with laser light at 532 nm under *in situ* Raman experiment.

TABLE 1. Ratios of Five Gaussian Components of OH Stretching Raman Bands and Degree of Non-Hydrogen-Bonded Water (DNHBW) for Various Pure Water

sample[a]	(1) 3018 cm^{-1} (%)	(2) 3223 cm^{-1} (%)	(3) 3393 cm^{-1} (%)	(4) 3506 cm^{-1} (%)	(5) 3624 cm^{-1} (%)	DNHBW (%)
a	5.29	40.22	33.20	15.66	5.63	21.29
b	5.26	40.17	33.33	15.40	5.83	21.24
c	3.93	38.31	33.65	16.78	7.33	24.11
d	1.19	35.30	33.20	20.36	9.95	30.31
e	5.23	39.72	33.54	15.71	5.80	21.50
f	2.78	37.18	33.81	18.97	7.26	26.23
g	4.59	37.96	33.1	17.57	6.78	24.36
h	3.70	38.24	33.82	17.84	6.29	24.23
i	4.09	38.76	32.97	17.29	6.89	24.17
j	4.86	39.44	32.83	16.77	6.09	22.86

[a] Various samples of pure water: (a) DI water; (b) CPT water; (c) AuNT water; (d) super SWC water; (e) AuNT water without illumination of light; (f) AuNT water prepared under illumination of green LED light; (g) AgNT water; (h) PtNT water, (i) Au/TiO_2NT water; (j) ORC-AuNT water.

AuNT water, except for the substitution of ceramic particles for Au NP-adsorbed ceramic particles. The super SWC was obtained by irradiating DI water-wetted Au NPs supported on ceramic particles with laser light at 532 nm *in situ* Raman spectrum measurement. These Raman spectra were further deconvoluted into five Gaussian sub-bands by using established literature methods. Although the exact band assignments are slightly different in the literature,[12,16−18] the consistent idea is that the bands on the low- and high-frequency sides are, respectively, related to strong and weak hydrogen-bonded OH features. In this work, the three components on the low-frequency side are assigned to hydrogen-bonded water, while the remaining two components on the high-frequency side are assigned to non-hydrogen-bonded water. The degree of non-hydrogen-bonded water (DNHBW) is defined as the ratio of the areas of the non-hydrogen-bonded OH stretching bands to the areas of the total stretching bands. This value is responsible for relating the free water molecules with their distinct properties distinguishable from bulk water with strong hydrogen bonds. As shown in Table 1, the values of DNHBW for DI, CPT, AuNT, and super SWC water, which are based on Figure 3, are 21.29 (21.37% for stored DI water after its preparation for 3 weeks), 21.24, 24.11, and 30.31%,

respectively. The average values of DNHBW for DI, CPT, AuNT, and super SWC water, based on three different batch experiments, are 21.35 ± 0.11, 21.31 ± 0.06, 24.27 ± 0.15, and 30.23 ± 0.10%, respectively. Compared to the significant differences between the values of DNHBW for the four water samples, the slight errors for these four individual values of DNHBW are acceptable. It suggests that this work is reproducible. The small difference between the values for fresh and stored DI water suggests 21.29% is a reliable reference value for bulk water used in DNHBW. The close values of 21.29 and 21.24% for the DI and CPT water, respectively, show that SWC water cannot be obtained by just using ceramic particles without the LSPR effect from the Au NPs. Encouragingly, the DNHBW can be significantly increased from 21.29 to 24.11% (an increase of ~13%) by utilizing the LSPR effect from the ceramic particle-supported Au NPs. This increase can be enhanced to 42% for super SWC. In this work, a SWC was prepared at a constant room temperature. However, the water film on particles is thin in recording the Raman spectrum of super SWC. Thus, the temperature of the irradiated water may be increased during the experiment, which may influence the corresponding Raman spectrum. To consider the influence of an increased temperature on the recorded Raman spectrum, a similar experiment was performed as for the measurement of the super SWC, but ceramic particle-supported Au NPs were replaced by ceramic particles—the value obtained for DNHBW was 21.65 ± 0.23%. Temperatures were monitored on the DI water-wetted ceramic particles with and without Au NPs in the two experiments under laser irradiation by using an IR thermometer (PK51C, accuracy ±1.5%) at a distance of 5 cm from the sample. The measured temperatures were 21.93 ± 0.06 and 21.77 ± 0.06 °C for DI water-wetted ceramic particles with and without Au NPs, respectively. The reduced difference in temperature suggests that the temperature effect can be ruled out for the observed extremely high DNHBW of the super SWC. Also, no asymmetric stretching vibration of the isolated water molecule was observed at ~3755 cm^{-1}, suggesting that water vapor can be excluded from this super SWC.[19] However, the observed DNHBW of 21.65 ± 0.23 for water-wetted ceramic particles, which is slightly higher than that of 21.35 ± 0.06% for DI water, might be ascribed to an interface effect on the hydrogen bonding of water on ceramic particles.

To further clarify that the preparation of SWC is from plasmonic absorption of light rather than from a simple thermal source sample of DI water, ceramic particle-treated water and Au-coated ceramic particle-treated water were also prepared at increased temperature of 50 °C and measured at room temperature after cooling. The corresponding values of DNHBW are 21.37, 21.36, and 21.35% for DI water, ceramic particle-treated water, and Au-coated ceramic particle-treated water, respectively, compared to values of DNHBW of 21.29, 21.24, and 24.11% for DI water, CPT water, and AuNT water (prepared at room temperature), respectively, indicating that joule heating does not contribute significantly to the successful preparation of SWCs. The ability of "hot" electrons, which come from Au NP surface plasmon decay, can drive the creation of SWCs. The large kinetic barriers encountered in creating SWCs prevent accessibility simply by injecting heat. A similar phenomenon has been shown in a study on a plasmonic water-splitting cell.[5] Two samples based on Fe_3O_4 NPs coated on ceramic particles were prepared. One of the experimental conditions was similar to that used in the preparation of AuNT water, but the Au NP-coated ceramic particles were replaced by Fe_3O_4 NP-coated ceramic particles. The other experimental condition was similar to that used in the preparation of super SWC, but the Au NP-coated ceramic particles were replaced by Fe_3O_4 NP-coated ceramic particles. The measured values of DNHBW were 21.23 and 21.61% for the former and the latter, respectively. As discussed before, the values 21.29, 24.11, and 30.31% were found for DI water, AuNT water, and super SWC, respectively. Similar values of 21.23 and 21.29% indicate that a surface coating on the NPs affecting the ability of the system to create SWC can be ruled out. However, the measured DNHBW of 21.61% for water-wetted Fe_3O_4 NP-coated ceramic particles (30.31% for water-wetted Au NP-coated ceramic particles), which is slightly higher than that of 21.29% for DI water, might be ascribed to an interface effect on the hydrogen bonding of water on Fe_3O_4 NP-coated ceramic particles. It also indicates that this interface effect on water would disappear after exfoliating water from the particles' surfaces.

Measured DNHBW values of 24.11, 23.52, 23.11, 22.11, and 21.39% were recorded for AuNT water after its preparation for 0, 1, 2, 3, and 5 days, respectively. Compared to the time scale (~10^{-12} s) normally ascribed to a dynamic equilibrium for hydrogen-bond breaking and re-formation in bulk water, this slow decay for the prepared AuNT water is interesting. Because the forward reaction from bulk water to AuNT water with weak hydrogen bonds is endergonic, the HET on the Au NPs under resonant illumination favors this forward reaction. In storage in the absence of Au NPs, both the forward and reverse reactions are slow due to the huge activation energies required for both reactions. In this work, the values of DNHBW are all located on the level of 24 for SWCs prepared by using NPs of Au, Ag, Pt, and Au/TiO_2 under the illumination of fluorescent lamps, as shown in Table 1. Although the distinct surface plasmon extinction bands are different for different NPs, the corresponding LSPR effects might be similar to these noble metal NPs with broad absorption bands over the whole visible light region when experiments were performed under illumination of

indoor fluorescent lamps. Moreover, these similar values of DNHBW for these different NPs of Au, Ag, Pt, and Au/TiO_2 suggest that the prepared SWC with a higher energy, compared to bulk water, is trapped in a relatively stable state in an activation energy valley, in which it can persist in liquid water without reverting to normal hydrogen-bonding patterns observed in bulk water. The distinct properties of the water, illuminated in the presence of Au NPs, persist after the illumination has ceased because the prepared SWC is in a new thermodynamic equilibrium state, which is distinguishable from that of bulk water. Compared to the reference value of DNHBW of 21.29% for DI water, the relatively higher value of DNHBW of 24.11% for AuNT water represents a macroscopic phenomenon for the AuNT water with a higher energy level, which is trapped in a relatively stable state in an activation energy valley. There is also the microscopic phenomenon of dynamic equilibrium between hydrogen-bond breaking and re-formation in water: this phenomenon is similar with that gas-phase water steam with small water clusters which is macroscopically stable in air at room temperature, while the microscopically dynamic equilibrium it possesses between hydrogen-bond breaking and re-formation is still maintained. In conclusion, different water samples with correspondingly different values of DNHBW, as shown in Table 1 and discussed in Supporting Information (SI), have confirmed the successful preparation of SWC by utilizing the LSPR effects. Sample e in Table 1 represents AuNT water without illumination of light, which was obtained by using the similar preparation condition used in the preparation of the AuNT water, but the experiment was performed in the dark. Compared to the values of DNHBW of 21.29% (DI water for a reference) and 24.11% (AuNT water), the values of DNHBW of 21.24% (CPT water) and 21.50% (AuNT water without illumination of light) suggest that both the Au NPs and the illumination of resonant light are necessary for the preparation of the SWC water. Meanwhile, the mixing process between AuNT water and DI water is a physical process, as indicated by the linear relationship between DNHBW and the percentage of AuNT water in the mixed water shown in Figure S1.

To further confirm the mechanism on the creation of SWC, coating the bare Au NPs with a dielectric coating of SiO_2 was performed. This coating would introduce a barrier to HET while keeping the localized heat source around the NP relatively unchanged. Therefore, we can directly probe whether the mechanism is due to localized thermal effects or solely to HET. Experimental results indicate that the values of DNHBW for DI water and $Au@SiO_2NT$ water are 21.37 and 21.94%, respectively. The $Au@SiO_2NT$ water was obtained by using preparation conditions similar to those used in the preparation of AuNT water under illumination of green LED, except for the substitution of Au NPs@SiO_2 nanocomposites (NCs) for Au NPs. Compared to DNHBW of 26.23% for AuNT water prepared under illumination of green LED, the slightly increased value of 21.94% ($Au@SiO_2NT$ water) from that of 21.37% (DI water) suggests that the mechanism of the creation of SWC is mainly due to HET.

We also carried out experiments on D_2O that are routinely done to assess the degree of hydrogen bonding in H_2O water. Although the hydrogen bond in D_2O is stronger than that in H_2O, the DNHBW can be also increased from 23.24 to 24.15% by utilizing the LSPR effect from the ceramic particle-supported Au NPs. This is an increase of ~3.9% in DNHBW. This increase can be enhanced to 7.6% for super SWC, as shown in Table S1 and Figure S2 (see SI for more details).

As reported in the literature,[20−22] light-induced vapor generation at water-immersed Au NPs is enabled when Au NPs are illuminated with solar energy or resonant light of sufficient intensity. However, the threshold of resonant light intensity is $\sim 10^6$ W m^{-2}. In this work, in preparation of SWCs with weak hydrogen bonding, DI water (pH 7.23, T = 23.5 °C) was allowed to flow through the glass tube (diameter of 3 cm) filled with Au NP-adsorbed ceramic particles (height of 15 cm) under illumination. Then the AuNT water (pH 7.25, T = 23.3 °C) was collected in glass sample bottles for subsequent measurements (all conducted within 2 h). Because the measured DNHBW values of 24.11 and 23.52% were recorded for AuNT water after its preparation for 0 and 1 days, respectively, its decay in SWCs was low after 1 day, as referred to a reference DNHBW value of 21.29% for DI water. Therefore, the maximum elapsed time, from sample preparation to measurement, of 2 h is acceptable. The Raman OH stretching spectrum of AuNT water was measured 3 min after the preparation of the sample; the corresponding DNHBW value was 24.54%, which is slightly higher than that of 24.11% for AuNT water (measured 2 h after the preparation of the sample). Illumination took place under a fluorescent lamp or a green LED with light power densities at 538 nm of $\sim 10^{-3}$ and 10^{-2} W m^{-2}, respectively—this being far lower than that required for light-induced vapor generation. The time for the water steam generation in the batch system is <5 s after the commencement of illumination.[20] In our continuous flowing system, the time for water flowing through the glass tube is ~1500 s. The energy density used in this work is still far lower than that for generating water steam shown in the literature. It is well-documented that the required heat for breaking the hydrogen bonds is 10−40 kJ mol^{-1}, which is lower than that of 136 kJ mol^{-1} for evaporating water at room temperature. In this work, the water temperature was not significantly changed when it passed through the glass tube with Au NPs under illumination. Therefore, the effect of HET for breaking the hydrogen bonds of bulk water can be achieved

under illumination with white light and further enhanced by wavelength-optimized resonant light. The energy efficiency, η, in the preparation of SWC under illumination of green LED was estimated from the ratio of the energy required for breaking the hydrogen bonds of bulk water to that provided from the light energy of LED, as defined below.

$$\eta = (E_{HB}M_{water})/(P_{LED}t) \times 100\% \quad (1)$$

where an energy of hydrogen bond, E_{HB}, of 20 kJ mol^{-1} was used. To obtain 75 g (or 75 cm^3, using a density of 1 g cm^{-3}) of SWC, the moles of bulk water, M_{water}, in which hydrogen bonds were broken, were calculated from the moles (4.2 mol) multiplied by the difference in values of DNHBW of DI water (21.29%) and AuNT water (26.23%) under the illumination of green LED. The LED power output (P_{LED}) was 16 W, and the illumination time, t, for 75 cm^3 DI water passing through the glass tube was ~1500 s. Therefore, the energy efficiency for the preparation of SWC under the illumination of green LED was approximately 17% (4.1 kJ/24 kJ): note that this value does not include energy losses from LED scattering and light penetration through the glass tube.

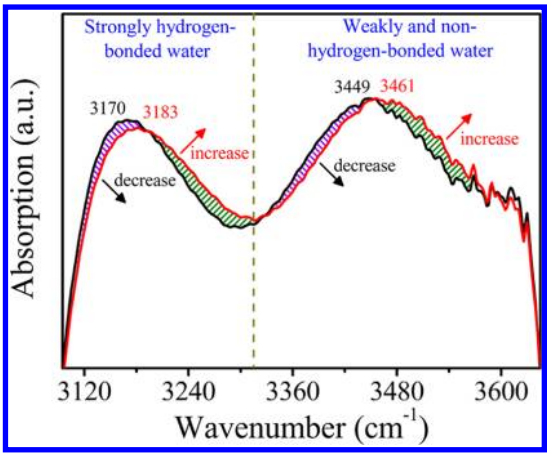

Figure 4. FTIR absorption spectra of OH stretching of DI water (black line) and AuNT water (red line).

FTIR spectra were also employed to confirm that AuNT water has weaker hydrogen bonds than DI water. As shown in Figure 4, there are two main hydrogen-bonding regions, that is, at approximately 3090 and 3640 cm^{-1}. The band in the region between 3090 and 3310 cm^{-1} corresponds to triply hydrogen-bonded (high-density hydrogen-bonded) water. The bands in the region between 3310 and 3640 cm^{-1} correspond to doubly, singly, and non- (free) hydrogen-bonded water.[23,24] Similarly, as discussed with regard to the Raman spectra, it is recognized that the bands on the low- and high-frequency sides are related to strongly and weakly hydrogen-bonded OH features, respectively.[13,23,24] Comparing the IR spectrum of AuNT water with that of DI water, it was found that the OH stretching frequencies shift from 3170 to a higher 3183 cm^{-1} and from 3449 to a higher 3461 cm^{-1} in the two main regions. The blue shifts observed with the AuNT water indicate a decrease in hydrogen-bonding strength,[10,23,24] which can be ascribed to the disordered structure of AuNT water with weaker hydrogen bonds. Moreover, the increases in the green shaded areas on the high-frequency sides and the decreases in the purple shaded areas on the low-frequency sides in the two main groups further confirm the generation of the water with markedly weaker hydrogen bonding.

Distinct Properties of Water with Reduced Hydrogen Bonding. As recently reported,[25] the electrochemical properties of phenols and quinones in organic solvents are strongly influenced by hydrogen bonding with water. Experiments were performed to highlight the properties attributable to the weak hydrogen bonding of AuNT water as distinct from bulk water. As shown in Figure 5A, the anodic peak of hydroquinone (HQ) cathodically shifts as the DI water content increases due to the hydrogen bonding of HQ with water. This result is consistent with the literature report cited above.[25] Encouragingly, as shown in Figure 5B, this cathodic shift is more significant with AuNT water, especially with AuNT water prepared under LED illumination. For example, with H_2O (0.206 M), the

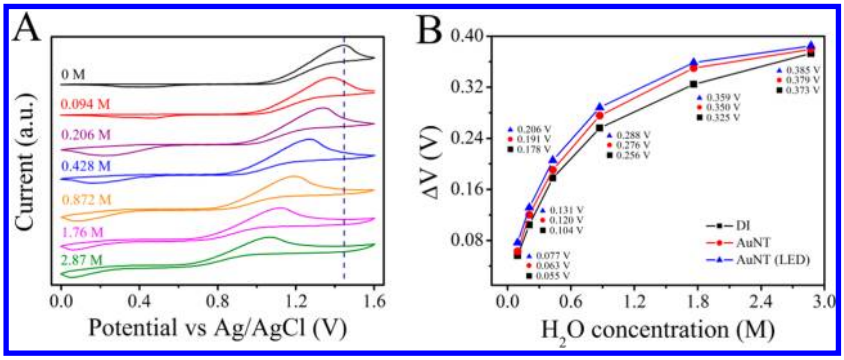

Figure 5. (A) Cyclic voltammograms of 2 × 10^{-3} M BQ in CH_3CN at various concentrations of DI water containing 5 × 10^{-3} M tetra-*n*-butylammonium hexafluorophosphate as the supporting electrolyte at a scan rate of 100 mV s^{-1} on a 2 mm diameter Pt electrode. (B) Cathodic shifts of anodic peaks in solutions containing various concentrations of different pure water; black square, red circle, and blue triangle represent DI water, AuNT water, and AuNT water prepared under illumination of green LED light, respectively.

cathodic shifts were enhanced by 15 and 26% (compared to DI water) when the experiments were performed using AuNT water prepared under a fluorescent lamp and LED, respectively. These interesting phenomena reveal that there is more "free water" in the AuNT water with weaker hydrogen bonding, which can strongly interact with HQ by hydrogen bonding. To calibrate the water contents of polyethylene glycol 400 (PEG400), DI water (10 wt %), and AuNT water, they were individually dissolved in PEG400. The measured water contents (Metrohm 870 KF Titrino plus) were 10.97 and 10.44 wt % for DI water and AuNT water, respectively. Because the AuNT water with weaker hydrogen bonding can form more hydrogen bonds with PEG, the measured content of available water was decreased by 4.8% (((10.97 − 10.44)/10.97) × 100%), as compared with DI water.

The AuNT water's weak hydrogen bonding is responsible for its distinct properties, which are significantly different from those of bulk water. As shown in Table S2, the saturated solubilities of NaCl, Tapimycin (an antibiotic), and the maximum content of dissolved O_2 in water can be significantly increased when DI water is replaced by AuNT water in experiments, especially for AuNT water prepared under LED illumination. The corresponding discussion is shown in SI. It is well-known that the saturated solubility of NaCl is difficult to increase by elevating the temperature of solution. The significant increases in the saturated solubility of NaCl and the maximum content of dissolved O_2 in AuNT water at ambient laboratory temperatures are interesting findings. Moreover, AuNT water with weaker hydrogen bonding is responsible for its higher saturated vapor pressure at room temperature; see Table S3 which indicates that the saturated vapor pressure of AuNT water is significantly higher than that of DI water (more discussion of this is shown in SI). In experiments, a static vapor−liquid−liquid equilibrium (VLLE) apparatus was used to measure the VLLE data. Before measurement, degassed solution was transferred into the equilibrium cell, in which the level of the vapor−liquid−liquid interface should be adjusted properly such that the upper liquid phase can be circulated. This distinct property of AuNT water also leads to a correspondingly fast evaporation rate, as shown in Figure S3. In evaporation experiments, DI water was individually added in two glass beakers, which were placed on a platform of an orbital shaker under illumination of a fluorescent lamp together. One beaker contained Au NP-adsorbed ceramic particles for the preparation of AuNT water. In the other beaker, there is no Au NP-adsorbed ceramic particle for a blank experiment performed in DI water. Moreover, compared to DI water, a shorter heating time from room temperature to boiling point in ambient laboratory atmosphere was observed for AuNT water. The corresponding discussion is shown in SI.

The contact angles of DI water (89.7° at beginning, 80.8° after 10 min) and AuNT water (83.5° at beginning, 44.9° after 10 min) on artificial skins are shown in Figure S4. It reveals that AuNT water, with its weaker hydrogen bonding, has less cohesion than DI water. This distinct property is also responsible for the contact angles of 47.9, 48.3, and 41.7° for DI, CPT, and AuNT water, respectively, on general glass slides. These results based on contact angles are consistent with those discussed in the context of Raman spectra above. Meanwhile, easy penetration into artificial skin was observed with AuNT water (more discussion is given in SI). The degree of swelling of the artificial skin with AuNT water was also examined. In experiments, two pieces of preweighted artificial skins were individually immersed in DI water and AuNT water for 1 h. Then the excess water on the surfaces of skins was quickly and slightly wiped off. Subsequently, the wet skins were weighed. As shown in Table S4, the degrees of swelling were 9.45 and 11.8% for DI water and AuNT water, respectively. This value was increased by 25% by using AuNT water. As revealed in a study focused on a bioinspired polymer composite actuator and generator driven by water gradients,[7] AuNT water has emerged as a promising candidate for further improvement of the water-driven actuator.

The chemical activity of the AuNT water, compared to DI water, was examined by the reduction of a Au-containing complex to Au NPs with the aid of natural chitosan (Ch) at room temperature, as shown in Figure S5. The corresponding discussion is shown in SI. The experimental results indicate that Au NPs can be successfully prepared with AuNT water as the reducing agent. This intriguing finding opens a new "green pathway" in chemical reduction.

Antioxidative Activity of Water with Reduced Hydrogen Bonding. It is well-known that hydroxyl radicals are the most cytotoxic ROS, and as such, they can directly or indirectly damage DNA.[26,27] The chemical activity of AuNT water as a reducing agent may offer a new therapy for scavenging free radicals. Figure 6 demonstrates the scavenging ability of AuNT water on hydroxyl radicals. The four ESR splitting signals shown in spectrum A are the characteristics of hydroxyl radicals.[14] As expected, as no ESR intensity differences are observed in spectra A and B, it is suggested that the chemical properties of CPT water and DI water are very similar. However, the production of hydroxyl radicals was significantly reduced in the presence of AuNT water with its weak hydrogen bonding; see spectrum C. The corresponding ESR intensity decreased by ~63%, as compared with that for an experiment performed in the presence of DI water. In calculating the average intensities, the two strongest peaks at ~3473 and 3488 G were used. As shown in the literature,[28,29] water can form a H_2O−OH radical complex through hydrogen bonding in the atmosphere.

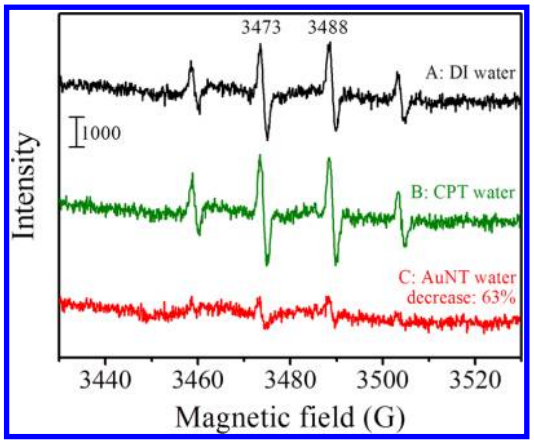

Figure 6. ESR spectra of hydroxyl free radicals based on various water. (A) DI water (black line) for reference; (B) ceramic particle-treated (CPT) water (green line), and (C) AuNT water (red line). The hydroxyl free radicals were obtained by using the well-known Fenton reaction, in which ferrous iron donates an electron to hydrogen peroxide to produce the hydroxyl free radical.

To the best of our knowledge, this antioxidative activity in scavenging free radicals from AuNT liquid water is the first report in the literature.

The ability of AuNT water in radical scavenging also demonstrates a positive effect on decreasing the corresponding ESR intensities of 2,2-diphenyl-1-picrylhydrazyl (DPPH) stable free radicals in solutions containing different contents of AuNT water, as shown in Figure 7. There is a linear relationship between the decrease of ESR intensity and the corresponding increased content of AuNT water. This also suggests that the mixing process of AuNT water with DI water belongs is a physical process, which does not change the chemical activity of AuNT water.

As shown in the literature,[30,31] biological studies focused on anti-inflammatory effects are generally performed by evaluating the ability to inhibit the production of nitric oxide (NO) by lipopolysaccharide (LPS)-activated monocytes/macrophages. Figure 8 shows the inflammation−preventive effect of AuNT water, compared to DI water, with respect to the reduction of LPS-induced NO release. Because the intracellular ROS level is closely associated with NO production in macrophage cells and AuNT water with antioxidative activity *in vitro*, an experiment was undertaken to determine the activity in cells. Stimulating macrophages with LPS caused a gradual nitrite release in cell culture medium with a dose-dependent manner. Nitrite monitoring was performed using the Griess reaction as isolated measurements at 24 h after the stimulation by LPS. The same experiments using cells with LPS stimulation were performed as ROS level indication. In order to evaluate the effect of AuNT water on activated macrophage cells, AuNT water and DI water-prepared Dulbecco's modified essential medium (DMEM) were compared for RAW 264.7

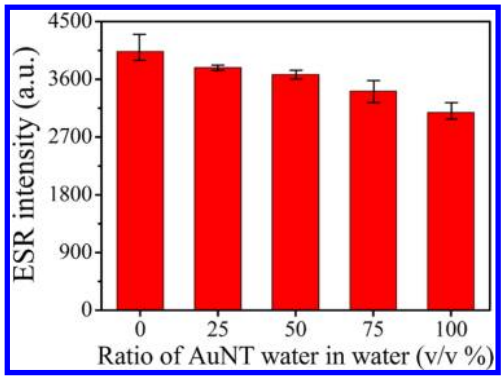

Figure 7. Scavenging of DPPH free radicals by using water composed of different ratios of AuNT water in water.

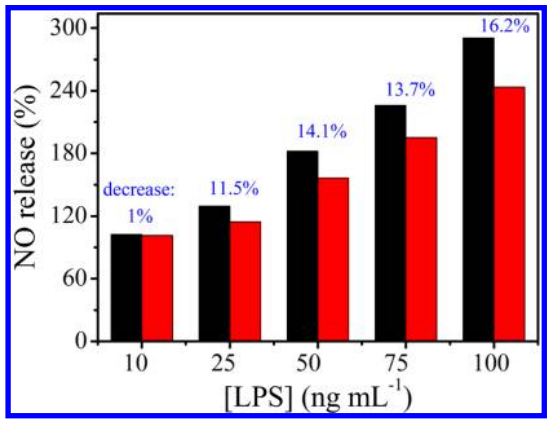

Figure 8. Antioxidative activity of AuNT water (red block) compared to DI water (black block) on reduction of LPS-induced NO release with dose of LPS. Determination of nitric oxide (NO) production was made following the method shown in the literature (see SI). DI water and AuNT water were used for medium preparation.

macrophage cell cultures with LPS stimulation (0−100 ng mL^{-1}). As shown in Figure 8, the NO production that stimulates macrophages with LPS was lower in AuNT water-prepared medium when compared to control DMEM medium. The elevated NO production levels were significantly decreased ($p < 0.05$; this p value means that the deviation probability of experimental data is less than 0.05, which indicates that the experimental result is significant) in AuNT water DMEM in the presence of 75 and 100 ng mL^{-1} LPS. Incubation with AuNT water−DMEM gives rise to suppression of NO release in LPS-activated macrophage cells.

CONCLUSION

We have successfully utilized the LSPR of noble metal NPs to prepare AuNT liquid water with SWCs. The value of DNHBW from Raman spectra of OH stretching is defined for SWCs with distinct properties. This innovative definition is successfully reflected on the corresponding performances of SWC with different values of DNHBW. The AuNT water at pH 7.25 exhibits distinct properties at room temperature, which are

significantly different from the well-known properties of bulk water at the same pH. The saturated solubilities of NaCl, Tapimycin, and the maximum content of dissolved O_2 in AuNT water compared to DI water can be significantly increased. Another example is its ability to scavenge free hydroxyl and DPPH radicals. Also, it effectively reduces NO release from LPS-induced inflammatory cells. These findings of AuNT water with distinct properties and antioxidative activity like gas water are the first shown in the literature. These make it applicable in water-related fields to investigate innovative aspects of effects from liquid SWC, such as efficient hydrogen production from water splitting and efficient hemodialysis.

MATERIALS AND METHODS

Chemicals and Materials. Electrolyte of NaCl and reagents of hydroquinone (HQ), 5,5-dimethyl-1-pyrroline *N*-oxide (DMPO), 2,2-diphenyl-1-picrylhydrazyl, and *Escherichia coli* lipopolysaccharide were purchased from Sigma-Aldrich Organics. Reagents of H_2O_2 and iron(II) chloride tetrahydrate were purchased from Acros Organics. Reagent of phosphate-buffered saline (PBS) was purchased from Bioman Organics. Reagent of ethylenediaminetetraacetic acid (EDTA) was purchased from Bioshop Organics. All of the reagents were used as received without further purification. Antibiotic of Tapimycin was purchased from Yung-Shin Pharm. Ind. Co., Ltd., Taiwan. The 40-mesh-screened ceramic particles (molar compositions: 92% SiO_2, 3.0% Na_2O and K_2O, 2.0% Fe_2O_3, 1.5% Al_2O_3, 0.5% CaO, 0.5% MgO, and other rare metal oxides) for filtering through drinking water were purchased from Chyuan-Bang Enterprise Co., Ltd., Taiwan. Commercial chitosan powders with a degree of deacetylation of 0.82 were purchased from First Chemical Works, Taiwan. All of the solutions were prepared using 18.2 MΩ cm deionized (DI) water provided from a Milli-Q system. All of the experiments were performed in an air-conditioned room at ~24 °C. The water temperature is ~23.5 °C.

Preparation of Au NPs. The Au NPs (~10 nm) in an aqueous solution were obtained from a Au sheet (purity of 0.9999) by using electrochemical and thermal reduction methods, as shown in our previous report.[32] Typically, the Au electrode was cycled in a deoxygenated aqueous solution of 40 mL containing 0.1 N NaCl and 1 g L^{-1} Ch from −0.28 to +1.22 V *vs* Ag/AgCl at 500 mV s^{-1} for 200 scans under slight stirring. The durations at the cathodic and anodic vertices are 10 and 5 s, respectively. Immediately, without changing the electrolytes, the solution was heated from room temperature to boiling at a heating rate of 6 °C min^{-1} in air. After the clear Au NP-containing solution was cooled, it was separated from the settlement of Ch. Then the Au NP-containing solution was placed in an ultrasonic bath for 30 min and was further centrifuged at 3600 rpm for 2 min to remove Ch to prepare pure Au NPs in solution.

Preparation of Au NP-Adsorbed Ceramic Particles. The rinsed ceramic particles were immersed in a solution containing 30 ppm Au NPs for 1 day. Then the Au NP-adsorbed ceramic particles were rinsed throughout with deionized water and finally dried in an oven at 100 °C for 1 day. Subsequently, the prepared Au NP-adsorbed ceramic particles were loaded in a valve-equipped glass tube (30 mm i.d., L = 300 mm). Before we prepared the AuNT water, the Au NP-adsorbed ceramic particles in the glass tube were rinsed with deionized water for several cycles until the pH values are almost identical (pH 7.23 and water temperature at ~23.5 °C) before and after it passed through the particle-loaded tube.

Conflict of Interest: The authors declare no competing financial interest.

Acknowledgment. The authors thank the National Science Council of ROC and Taipei Medical University for their financial support.

Supporting Information Available: Other experimental methods and additional discussions, Tables S1−S4 and Figures S1−S5. This material is available free of charge *via* the Internet at http://pubs.acs.org.

REFERENCES AND NOTES

1. Li, J. F.; Huang, Y. F.; Ding, Y.; Yang, Z. L.; Li, S. B.; Zhou, X. S.; Fan, F. R.; Zhang, W.; Zhou, Z. Y.; Wu, D. Y.; *et al.* Shell-Isolated Nanoparticle-Enhanced Raman Spectroscopy. *Nature* **2010**, *464*, 392–395.
2. Lim, D. K.; Jeon, K. S.; Hwang, J. H.; Kim, H.; Kwon, S.; Suh, Y. D.; Nam, J. M. Highly Uniform and Reproducible Surface-Enhanced Raman Scattering from DNA-Tailorable Nanoparticles with 1-nm Interior Gap. *Nat. Nanotechnol.* **2011**, *6*, 452–460.
3. Gobin, A. M.; Lee, M. H.; Halas, N. J.; James, W. D.; Drezek, R. A.; West, J. L. Near-Infrared Resonant Nanoshells for Combined Optical Imaging and Photothermal Cancer Therapy. *Nano Lett.* **2007**, *7*, 1929–1934.
4. Turner, J. A. Sustainable Hydrogen Production. *Science* **2004**, *305*, 972–974.
5. Lee, M. J.; Ji, S.; Stucky, X. G. D.; Moskovits, M. Plasmonic Photoanodes for Solar Water Splitting with Visible Light. *Nano Lett.* **2012**, *12*, 5014–5019.
6. Fratzl, P.; Barth, F. G. Biomaterial Systems for Mechanosensing and Actuation. *Nature* **2009**, *462*, 442–448.
7. Ma, M.; Guo, L.; Anderson, D. G.; Langer, R. Bio-inspired Polymer Composite Actuator and Generator Driven by Water Gradients. *Science* **2013**, *339*, 186–189.
8. Murata, K.; Mitsuoka, K.; Hirai, T.; Walz, T.; Agre, P.; Heymann, J. B.; Engel, A.; Fujiyoshi, Y. Structural Determinants of Water Permeation through Aquaporin-1. *Nature* **2000**, *407*, 599–605.
9. Stamenkovic, V. R.; Fowler, B.; Mun, B. S.; Wang, G.; Ross, P. N.; Lucas, C. A.; Marković, N. M. Improved Oxygen Reduction Activity on Pt3Ni(111) *via* Increased Surface Site Availability. *Science* **2007**, *315*, 493–497.
10. Vöhringer-Martinez, E.; Hansmann, B.; Hernandez, H.; Francisco, J. S.; Troe, J.; Abel, B. Water Catalysis of a Radical-Molecule Gas-Phase Reaction. *Science* **2007**, *315*, 497–501.
11. Shultz, M. J.; Vu, T. H.; Meyer, B.; Bisson, P. Water: A Responsive Small Molecule. *Acc. Chem. Res.* **2012**, *45*, 15–22.
12. David, J. G.; Gierszal, K. P.; Wang, P.; Ben-Amotz, D. Water Structural Transformation at Molecular Hydrophobic Interfaces. *Nature* **2012**, *491*, 582–585.
13. Scatena, L. F.; Brown, M. G.; Richmond, G. L. Water at Hydrophobic Surfaces: Weak Hydrogen Bonding and Strong Orientation Effects. *Science* **2001**, *292*, 908–912.
14. Ohsawa, I.; Ishikawa, M.; Takahashi, K.; Watanabe, M.; Nishimaki, K.; Yamagata, K.; Katsura, K.; Katayama, Y.; Asoh, S.; Ohta, S. Hydrogen Acts as a Therapeutic Antioxidant by Selectively Reducing Cytotoxic Oxygen Radicals. *Nat. Med.* **2007**, *13*, 688–694.
15. Sohal, R. S.; Weindruch, R. Oxidative Stress, Caloric Restriction, and Aging. *Science* **1996**, *273*, 59–63.
16. Li, R.; Jiang, Z.; Guan, Y.; Yang, H.; Liu, B. Effects of Metal Ion on the Water Structure Studied by the Raman O−H Stretching Spectrum. *J. Raman Spectrosc.* **2009**, *40*, 1200–1204.
17. Carey, D. M.; Korenowski, G. M. Measurement of the Raman Spectrum of Liquid Water. *J. Chem. Phys.* **1998**, *108*, 2669–2775.
18. Tomlinson-Phillips, J.; Davis, J.; Ben-Amotz, D. Structure and Dynamics of Water Dangling OH Bonds in Hydrophobic Hydration Shells. Comparison of Simulation and Experiment. *J. Phys. Chem. A* **2011**, *115*, 6177–6183.

19. Senior, W. A.; Thompson, W. K. Assignment of Infra-red and Raman Bands of Liquid Water. *Nature* **1965**, *205*, 170.
20. Neumann, O.; Urban, A. S.; Day, J.; La, S.; Nordlander, P.; Halas, N. J. Solar Vapor Generation Enabled by Nanoparticles. *ACS Nano* **2013**, *7*, 42–49.
21. Fang, Z.; Zhen, Y. R.; Neumann, O.; Polman, A.; García de Abajo, F. J.; Nordlander, P.; Halas, N. J. Evolution of Light-Induced Vapor Generation at a Liquid-Immersed Metallic Nanoparticle. *Nano Lett.* **2013**, *13*, 1736–1742.
22. Polman, A. Solar Steam Nanobubbles. *ACS Nano* **2013**, *7*, 15–18.
23. Chan, R. H.; Bogomolni, R. A. Structural Water Cluster as a Possible Proton Acceptor in the Adduct Decay Reaction of Oat Phototropin 1 LOV2 Domain. *J. Phys. Chem. B* **2012**, *116*, 10609–10616.
24. Laporta, M.; Pegoraro, M.; Zanderighi, L. Perfluorosulfonated Membrane (Nafion): FT-IR Study of the State of Water with Increasing Humidity. *Phys. Chem. Chem. Phys.* **1999**, *1*, 4619–4628.
25. Tessensohn, M. E.; Hirao, H.; Webster, R. D. Electrochemical Properties of Phenols and Quinones in Organic Solvents Are Strongly Influenced by Hydrogen-Bonding with Water. *J. Phys. Chem. C* **2013**, *117*, 1081–1090.
26. Imlay, J. A. Cellular Defenses Against Superoxide and Hydrogen Peroxide. *Annu. Rev. Biochem.* **2008**, *77*, 755–756.
27. Yamada, M.; Shimizu, M.; Katafuchi, A.; Grúz, P.; Fujii, S.; Usui, Y.; Fuchs, R. P.; Nohmi, T. *Escherichia coli* DNA Polymerase III Is Responsible for the High Level of Spontaneous Mutations in MutT Strains. *Mol. Microbiol.* **2012**, *86*, 1364–1375.
28. Ohshima, Y.; Sato, K.; Sumiyoshi, Y.; Endo, Y. Rotational Spectrum and Hydrogen Bonding of the H_2O-HO Radical Complex. *J. Am. Chem. Soc.* **2005**, *127*, 1108–1109.
29. Allodi, M. A.; Dunn, M. E.; Livada, J.; Kirschner, K. N.; Shields, G. C. Do Hydroxyl Radical-Water Clusters, $OH(H_2O)_n$, n=1−5, Exist in the Atmosphere? *J. Phys. Chem. A* **2006**, *110*, 13283–13289.
30. Lee, T. S.; Chau, L. Y. Heme Oxygenase-1 Mediates the Anti-inflammatory Effect of Interleukin-10 in Mice. *Nat. Med.* **2002**, *8*, 240–246.
31. Meng, X. L.; Yang, J. Y.; Chen, G. L.; Zhanga, L. J.; Wanga, L. H.; Jie, L. J.; Wang, J. M.; Wu, C. F. RV09, a Novel Resveratrol Analogue, Inhibits NO and TNF-α Production by LPS-Activated Microglia. *Int. Immunopharmacol.* **2008**, *8*, 1074–1082.
32. Yu, C. C.; Liu, Y. C.; Yang, K. H.; Tsai, H. Y. Simple Method To Prepare Size-Controllable Gold Nanoparticles in Solutions and Their Applications on Surface-Enhanced Raman Scattering. *J. Raman Spectrosc.* **2011**, *42*, 621–625.